Solvent Pre-treated Effects of Carbon Nanotube-supported Cobalt Catalysts on Activity and Selectivity of Fischer-Tropsch Synthesis

Ali Karimi[1,*], Ali Mohajeri[1], Ali Jebreili Jolodar[2], Ali Morad Rashidi[1], and Khaled Forsat[1]

[1] Gas Research Division, Research Institute of Petroleum Industry, (RIPI) Tehran, Iran
[2] Process Development and Design, Research Institute of Petroleum Industry, (RIPI) Tehran, Iran

ABSTRACT

In this study, the effect of preparation technique of carbon nanotube (CNT)-supported cobalt catalysts on the activity and selectivity of Fischer-Tropsch synthesis (FTS) was studied. Different concentrations of acetic acid were used for the pretreatment of the catalyst support to modify the surface properties of CNT. This modification improved the reduction degree and dispersion of supported cobalt simultaneously. The catalysts were prepared by incipient wetness impregnation of the cobalt precursor, and deionized water was used as the preparation medium. The obtained catalysts were characterized by XRD, TPR, TEM, and H_2 chemisorption. The catalysts prepared under the optimum conditions exhibited significant stability and activity for FTS reaction in a CSTR reactor during 120 hr of experimental tests.

Keywords: Carbon Nanotube, Cobalt Catalyst, Fischer–Tropsch Synthesis, Acetic Acid, Functional Groups

INTRODUCTION

There is a renewed interest in Fischer-Tropsch synthesis (FTS) in both academic and industry, largely as a result of the demand for clean and renewable transportation fuel [1]. In the FTS reaction, syngas (a mixture of CO and H_2) is converted into liquid fuel via catalytic surface polymerization, which leads to a large variety of products such as paraffins, olefins, alcohols, and aldehydes [1-3]. Supported cobalt catalysts are well-known for their activity and selectivity towards FTS. High chain growth probability, lower deactivation rates, low water-gas shift activity, and low costs make cobalt catalysts the best candidates for converting syngas to clean liquid fuels [4, 5].

The FTS activity of cobalt catalysts depends solely on the number of active sites located on the surface of the support, formed by reduction. The number of active sites can be determined by the Co particle size dispersions, loading amount, and reduction degree [6, 7].

Preparing impregnated catalyst is actually a complex process, in which many individual steps might influence the final performance of the catalyst, i.e. metal precursor, solvent, carrier, aging time, drying time/temperature, and calcination temperature. Failure to control these parameters might lead to irreproducible catalyst preparation.

In order to achieve high surface active sites (Co^o), cobalt precursors are dispersed on porous carriers,

***Corresponding author**
Ali Karimi
Email: karimial@ripi.ir
Tel: +98 21 48252395
Fax: +98 21 44739716

Article history
Received: February 10, 2015
Received in revised form: July 05, 2015
Accepted: July 06, 2015
Available online: January 23, 2016

with SiO_2, Al_2O_3, and to a lesser extent TiO_2 being the most frequently used [5,8-9]. A drawback of these support materials is their reactivity toward cobalt, which, during preparation or catalysis, results in the formation of mixed compounds that are reducible only at high reduction temperatures [5, 8, 9]. To avoid these problems, the use of carbon as a support has been explored [10-12]. Activated carbon has many advantages including resistance to acidic or basic media, stable at high temperatures, etc., if utilized as a FTS catalyst support. Carbon nanotube (CNT) possesses similar properties and in most cases outperforms activated carbon for FTS [12]. CNT has many unique structural properties and have attracted increasing attention as a novel support medium for heterogeneous catalysis [8–14].

In CNT-supported cobalt catalyst, the strong metal-support interactions are reduced to a large extent [2]. The synthesis of highly dispersed and stable cobalt catalyst requires strong interactions between the support and the Co precursor [15]. It is considered that solvents, which are applied to pretreating the supports, remarkably influence the interaction between the cobalt and CNT supports; meanwhile, the groups from solvents, formed on the surface of supports, prohibit the sintering of supported cobalt [16–18]. The presence of functional groups on CNT surface gives rise to cation-exchange properties, which can act as anchor sites for the metal particles [17]. It seems that the formation of functional groups on CNT surface also accelerates the hydrogen spill-over effect in the reduction process. Furthermore, the concentration, distribution, and nature of hydroxyl groups on the CNT surface will increase the percentage dispersion, reduction degree, stability, and performance of these catalysts simultaneously [17].

In the present work, different concentrations of acetic acid used to pretreating the CNT support before the impregnation of cobalt precursors. Acetic acid should modify the properties of CNT surface such as the nature of hydroxyl and carboxyl groups, which results in a catalyst with different properties in comparison with the cobalt catalyst on common CNT.

EXPERIMENTAL PROCEDURES

Preparation of CNT Support

CNT was synthesized through methane decomposition at 900 °C over nanoporous magnesium oxide (Co-Mo/MgO) supported on cobalt-molybdenum nanoparticles by a chemical vapor deposition (CVD) process [20]. The reaction of methane decomposition was conducted at atmospheric pressure with a holding time of 20-50 min. The purification procedure was done as follows: the pristine CNT sample was added to an 18% HCl solution and mixed for about 16 hrs at ambient temperature. The resulting mixture was filtered and washed with distilled water. In order to achieve extra- purification, the prepared materials dissolved in 6 M nitric acid for 3 hrs at 70°C. After that, the washing step was repeated as mentioned above for the HNO_3 treatment process. The resulting cake dried at ambient temperature through the night.

Catalyst Preparation

The produced CNT with specific surface area, pore volume, and average pore diameter of 255 m^2/gr, 0.73 cm^3/gr, and 12 nm respectively, was used as the support in this study. The CNT was pretreated with 20, 60, and 90 wt.% acetic acid for 1 hr at room temperature by an incipient wetness impregnation method. The samples were then dried in air at 100 °C for 12 hrs [15].

The pretreated CNT support was impregnated with an aqueous solution of cobalt nitrate by an incipient wetness method. The loading of cobalt was 15 wt. % for all the catalysts. The cobalt CNT-supported catalyst with same loadings of cobalt and procedure was prepared on CNT without pretreatment, and was used as a reference.

All the catalysts were dried in air at 100 °C for 12 hrs, and calcined at 400 °C for 3 hr at a heating rate of 1

°C/min under argon (Ar) flow and slowly exposed to an oxygen atmosphere during the cooling step.

Catalyst Characterization

The cobalt loading and composition of catalysts were verified by an inductively coupled plasma (ICP) AES system.

The morphology of CNT and pretreated CNT-supported catalysts (Co-20AC, Co-60AC, Co-95AC, and Co-CNT) were characterized by transmission electron microscopy (TEM). The sample specimens for TEM studies were prepared by ultrasonic dispersion of the catalysts in ethanol, and the suspensions were dropped onto a carbon-coated copper grid. The TEM investigations were carried out using a Philips CM120 (100 kV) transmission electron microscope equipped with a NARON energy-dispersive spectrometer with a germanium detector.

The surface area, pore volume, and average pore radius of the CNT and all the catalysts were measured by an ASAP-2010 system from Micromeritics. The samples were degassed at 200 °C for 4 hrs under a 50 mTorr vacuum and their BET area, pore volume, and average pore radius were determined.

The XRD measurements of the CNT and the calcined catalysts were conducted with a Philips PW1840 X-ray diffractometer with monochromatized Cu/Kα radiation. Using the Scherrer equation, the average size of the Co_3O_4 crystallites in the calcined catalysts was estimated from the line broadening of a Co_3O_4 at 2θ of 36.88°. A *K* factor of 0.89 was used in the Scherrer formula. The Co_3O_4 particle size was converted to the corresponding cobalt metal particle size according to the relative molar volumes of metallic cobalt and Co_3O_4. The resulting conversion factor for the diameter of a given Co_3O_4 particle $d_{Co_3O_4}$ being reduced to metallic cobalt is [22]:

$$d_{Co^o}(nm) = 0.75 \times d_{Co_3O_4} \quad (1)$$

The amount of chemisorbed hydrogen (H_2) on the catalysts was measured using the Micromeritics TPD-TPR 2900 system. 0.25 gr of the calcined catalyst was reduced under H_2 flow at 400 °C for 20 hr and was then cooled to 70 °C under an H_2 flow. Then, the flow was switched to Ar at the same temperature; this step, which was used to remove the physisorbed H_2, lasted for about 30 minutes. The subsequent temperature programmed desorption (TPD) of the samples was obtained by increasing the temperature of the samples to 400 °C at a rate of 20 °C/min under an Ar flow. The resulting TPD spectra were used to determine the cobalt dispersion and its surface average crystallite size. The percentage of the dispersion and particle diameter are calculated by the Equations 2-5 [23].

Catalyst Activity Test

The catalysts were evaluated in terms of their FTS activity (gr HC produced/gr cat. /hr) and selectivity (the percentage of the converted CO that appears as a hydrocarbon product) in Temperature Programmed Reduction (TPR) spectra of the catalysts were recorded using a Micromeritics TPD–TPR 2900 system equipped with a thermal conductivity detector. The catalyst samples were first purged under a flow of argon at 400 °C to remove traces of water, and were then cooled to 40 °C. The TPR of 50 mg of each sample was performed using 5% hydrogen in an argon gas mixture at a flow rate of 40 cm^3/min. The samples were heated from 40 to 900 °C at a heating rate of 10 °C/min.

A continuous stirred tank reactor (CSTR) from Autoclave Engineers used, as shown in Figure 1, was used. The total volume of CSTR was 1 liter. The reactor was initially filled with cobalt catalyst, which crushed to a particle size smaller than 44 μm (325 ASTM mesh). The catalyst is reduced inside the reactor (in situ reduction) by hydrogen at 400 °C, a ramp rate of 2 °C/min, atmospheric pressure, and a space velocity of 1188 (N cm^3 $grcat.^{-1}$ hr^{-1}). The reduction vessel (reactor) was held at 400 °C for 24 hrs and then pressurized

with hydrogen and cooled to a specified reaction temperature.

$$\text{Calibration Value (lit. gas/area unit)}=\frac{\text{Loop Volume}\times\%\text{ Analytical gas}}{\text{Mean Calibration Area}} \quad (2)$$

$$H_2\text{ Uptake (moles/gr. cat.)}=\frac{\text{Analytical Area from TPD}\times\text{Mole of }H_2\text{ from calibration}}{\text{Mean Calibration Area}} \quad (3)$$

$$\%\text{ Dispersion}=\frac{H_2\text{ uptake}\times\text{Atomic weight}\times\text{Stoichiometry}}{\%\text{ Metal}}=\frac{\text{Number of Co atoms on surface}}{\text{Number of Co atoms in sample}}\times 100 \quad (4)$$

$$\text{Diameter}=\frac{6000}{\text{Density}\times\text{Specific surface area}\times\text{Dispersion}}\times 100 \quad (5)$$

Afterward, 350 gr of Merck paraffin wax (Merck index 1.07358, sulphate b0.015%) was degassed using a hydrogen flow at 100 °C and then added to the reduced catalyst under hydrogen atmosphere, in which the finely crushed cobalt catalyst was slurried with the liquid wax to produce a 12.5 wt.% suspension based on the unreduced catalyst. Inside the reactor, the mixture of liquid wax and catalyst particles is well mixed by a magnetically driven turbine agitator at 2000 rpm. Therefore, the solid phase is completely suspended in the liquid phase. The feed gas composed of H_2 (N99.999% purity) and CO (N99.995% purity), where they were taken from the cylinder. Their flow rates controlled by two mass flow controllers (Type 5850E, Brooks Instruments Div.). For decomposing carbonyls possibly present in the CO, the syngas is passed through a bed of carbonyl trap. Also, before entering the reactor, the feed is passed through a static mixer and then preheated up to near the reaction temperature. The slurry reactor is operated in a semibatch mode, in which syngas is continuously sparged to the slurry and volatile products are removed overhead. The gas outlet of the reactor is connected to a hot receiver (353 K) and then a cold receiver (273 K) at the system pressure. High molecular weight products are collected in the hot receiver and the remaining condensable materials are collected in the cold receiver for a typically period of 15-20 hrs during a steady state of the reactor system. In each receiver, the collected liquid products separated into an oil phase, which contained hydrocarbons, and aqueous phase, which consisted of water plus oxygenates. The gas stream leaving the cold receiver (unreacted gases H_2, and CO and non-condensed products containing C_1-C_5) passed through the back pressure regulator (Type 5866, Brooks Instruments Div.), where the pressure is reduced to a value slightly above atmospheric, and then to either an on-line GC or the vent line. The flow rate of the tail gas is measured using a wet gas flow meter. After changing the reaction conditions, the reactor operates about 12 hrs to ensure steady state operations are reached. The out gas was analyzed by a gas chromatograph (Varian CP-3800) equipped with TCD and FID detectors. The CO, CO_2, N_2, and O_2 were analyzed through two packed columns in series (Molecular sieve 13× CP 81025 with 2 m length, and 3 mm OD, and Hayesep Q CP1069 with 4 m length, and 3 mm OD) connected to a TCD detector. The C_1-C_5 hydrocarbons were analyzed via a capillary column (CP fused silica with 25 m×0.25 mm×0.2 μm film thickness) connected to an FID detector. Hydrogen was analyzed through Shimatzu, GC PTF 4C, equipped with a TCD detector and two columns in series (Propack-Q with 2m length, and 3 mm OD for CO_2, C_2H_4, and C_2H_6 separation and molecular sieve-5A with 2 m length, and 3 mm OD for CO, N_2, CH_4, and O_2 separation), which were connected to each other via a three way valve.

Argon was used as carrier gas with 25 cc/min flow. The collected liquid (Including hydrocarbons and oxygenates) were analyzed offline with Varian CP-3800 gas chromatograph equipped with capillary column (TM DH fused silica capillary column, PETRO COL 100 m×0.25 mm×0.5 µm film thickness) connected to an FID detector. The carrier gas was He and temperature programming was up to 260 °C .

Both total mass and atomic material balances were performed with the consideration that a run could be accepted for further analysis, if the oxygen material balance closed between 97 and 103%, otherwise the run was rejected. This criterion was adopted, since compounds containing carbon and hydrogen may accumulate in the reactor, in the form of high molecular weight hydrocarbons.

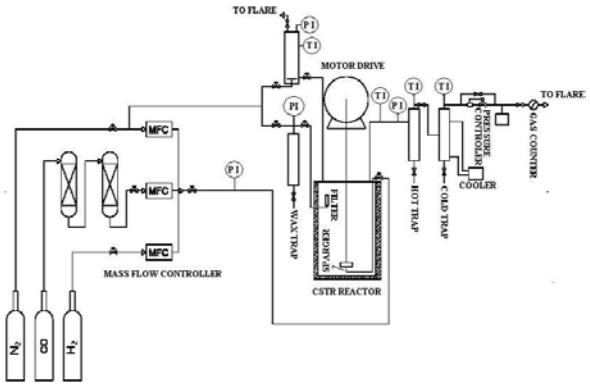

Figure 1: Experimental setup.

The mixed gases entered through a dip tube to the bottom of the CSTR below the stirrer. The CSTR was operated at 750 rpm. The temperature of the reactor was controlled via a PID temperature controller. The synthesis gas at a flow rate of 90 NL/hr (with an H_2/CO ratio of 2) was introduced and the reactor pressure was increased to 2.5 MPa. The reactor temperature was then increased to 220 °C at a rate of 1 °C/min. The products were continuously removed from the vapor and passed through two traps, namely one maintained at 100 °C (hot trap) and the other at 0 °C (cold trap). The uncondensed vapor stream was reduced to atmospheric pressure through a pressure letdown valve.

The accumulated reactor liquid wax products were removed every 12 hrs by passing through a 2 µm sintered metal filter located above the liquid level in the CSTR. Moreover, the contents of hot and cold traps removed every 12 hr, the hydrocarbon and water fractions separated and the collected liquid (Including hydrocarbons and oxygenates) were analyzed offline with Varian CP-3800 gas chromatograph equipped with a capillary column (TM DH fused silica capillary column, PETRO COL 100 m×0.25 mm×0.5 µm film thickness) connected to an FID detector. Both total mass and atomic material balances were performed with the consideration that a run could be accepted for further analysis, if the carbon material balance closed between 97 and 103%. This criterion was adopted, since compounds containing carbon and hydrogen may accumulate in the reactor, in the form of high molecular weight hydrocarbons. The conversion percentage of CO based on the fraction of CO forming carbon-containing products was calculated according to the below equation:

$$\text{CO conversion} = \frac{F_{in} \times M_{CO,in} - F_{out} \times M_{CO,out}}{F_{in} \times M_{CO,in}} \times 100 \quad (6)$$

where, F_{in}, $M_{CO,in}$, and F_{out}, $M_{CO,out}$ are the feed molar flow, the mole percentage of CO in the syngas feed, the product molar flow, and the mole percentage of CO in the product gas respectively.

FTS rate (gr HC/gr cat. /hr) is equal to weight of hydrocarbons (gr) produced in the reaction and defined as:

$$FTS\ rate = \frac{\sum F_{out} \times M_i \times MW_i}{gram\,of\ catalyst} \quad (7)$$

where, M_i and MW_i are the mole percentage and molecular weight of product *i* respectively.

The selectivity of product *i* (the percentage of the converted CO that appears as a given product), is based on the total number of carbon atoms in the product and therefore is defined as:

$$Selectivity\ of\ product\ i = \frac{n_i \times M_i}{\sum n_i \times M_i} \times 100 \quad (8)$$

n_i is the number of carbon atoms in product *i.*

The C_5^+ selectivity is the total selectivity of C_5 and hydrocarbons of a higher molecular weight.

According to chromatogram of the GC analysis, the olefin to paraffin ratio of hydrocarbons is defined as follows:

$$Olefin\ to\ Paraffin\ ratio\ of\ product\ i\ (i \geq 2) = \frac{Molar\ sum\ of\ olefin\ isomers\ of\ product\ i}{Molar\ sum\ of\ paraffin\ isomers\ of\ product\ i} \quad (9)$$

RESULT AND DISCUSSION

CNT Characterization

The produced CNT was purified by acid washing and drying steps and characterized by different methods. Figure 2 shows the SEM and TEM configuration of the as-grown CNT prepared by the CVD method [20, 24].

The pretreated CNT was characterized with FTIR technique performed by a Bruker ISS-88 instrument, whose spectrum is shown in Figure 3. For the modified CNT, the bands around 1570 and 1720 are attributed to the graphitic structure of CNT and the carboxyl group (-COOH).The presence of C–O (1118 cm^{-1}) and O-H (2400–3400 cm^{-1}) vibrations in the spectrum of the pretreated CNT were observed, which introduced to the tip and sidewalls of the CNT [21].

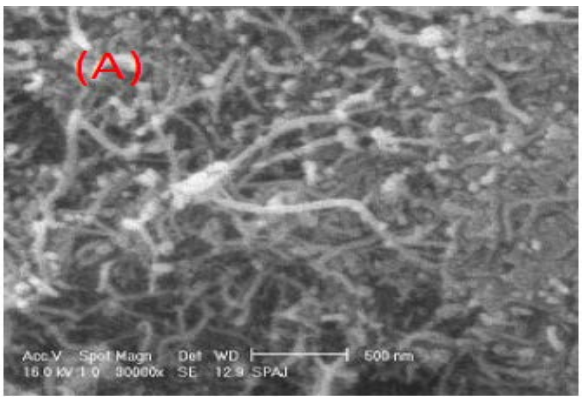

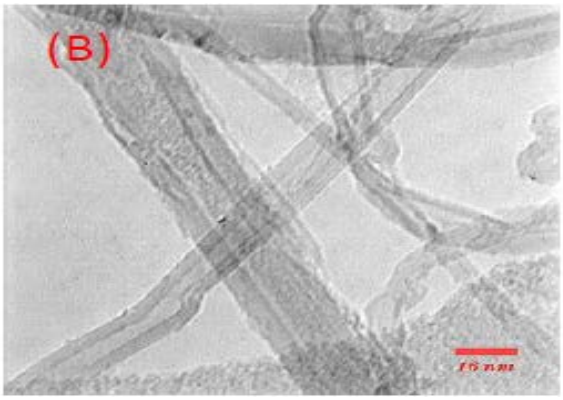

Figure 2: A) SEM image of CNT and B) TEM image of CNT.

Catalyst Characterization

The supported cobalt particle sizes for various catalysts were determined by TEM, XRD, and H_2 chemisorption. The activity of the cobalt catalyst in FTS depends solely on the number of active sites located on the surface of CNT formed by reduction. The number of active sites is determined by the cobalt particle size, loading amount, and the reduction degree [25]. Chen et al. observed that particle size was not the only property to have an effect on the FTS activity [26].

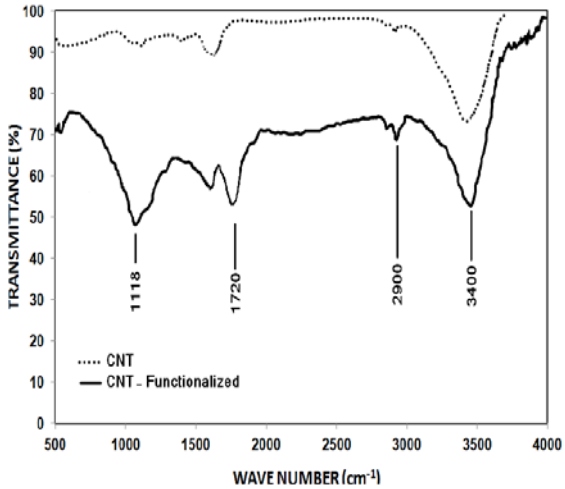

Figure 3: FTIR spectrum of CNT and acetic acid pretreated CNT.

The TEM images of the catalysts are shown in Figure 4; it demonstrates the dispersion of the particles made on acetic acid pretreated CNT and shows the particles that are inside and outside the CNT. In our case, the particles are mostly inside the CNT walls for the Co-60AC

(Figure 4). Due to the pretreatment of CNT support, the cobalt dispersion on catalyst surface increased and capillary forces led to the confinement of cobalt particles inside the CNT pores [20, 27-30]. The Co-95AC and Co-20AC catalysts particles were dispersed inside the tubes walls so that the percentage of the particles lying at the outer surface of the CNT walls was lower compared with the other catalysts prepared on a common CNT. Indeed, the narrow inner diameter of the CNT channels (9-10 nm) restricted the insertion of particles in sizes close to the channel diameter. Similar to previous works [31, 32] and as shown in the TEM images of the Co-CNT catalyst, the smaller cobalt particles are lying inside the CNT channels and the larger particles on the outside. The CNT channels have restricted the growth of the particles inside the tubes from 4 to 9 nm. Almost all the particles of sizes of 10 nm and higher were lying on the outer surface of the CNT walls.

Figure 5 depicts the size distribution of the cobalt particles, which was determined using the population of the total cobalt particles of each catalyst based on the data taken from different TEM images (four images were presented in Figure 4). This figure shows that the size of cobalt nanoparticles on pretreated CNT is higher than the ones supported on common CNT. Moreover, with the pretreated CNT, a narrow cobalt nanoparticle size distribution (6-9 nm) was obtained, because the surface functional groups act as sites of interaction with metal precursor [25]. Indeed, these data and TPR results confirm each other. According to Figure 5, the average particle size for catalyst with 15 wt.% cobalt loading, prepared on common CNT (Co-CNT) is equal to or larger than 6-11 nm. This result is in accordance with previous works [23, 28, 29].

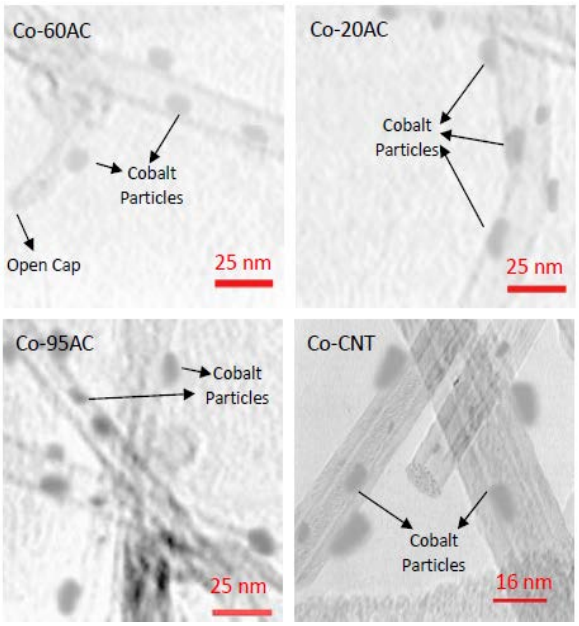

Figure 4: TEM images of the calcined catalysts.

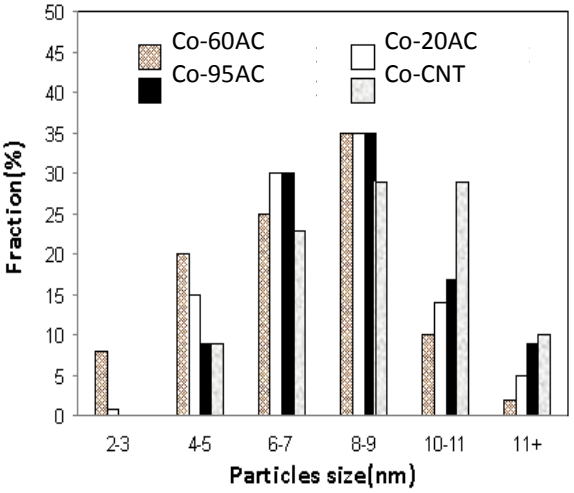

Figure 5: Particles size distributions for the calcined catalysts

The XRD patterns of various calcined catalysts are shown in Figure 6. The cobalt crystalline size of Co-CNT catalyst was the largest, as shown in Table 1 and Figure 6. The other catalysts, prepared by acetic acid pretreated CNT supports, also exhibited smaller cobalt particle size than Co-CNT according to H_2 chemisorption data presented in Table 1.

With reference to Figure 3, it was deduced that several kinds of functional groups same as hydroxyl, carboxyl (the -COOH), carbonyl (-C=O), and ester were positioned on the CNT surface. The FTIR peak at 2900 cm^{-1} shows the formation of C-H aliphatic hydrogen and the C-O stretching

band at 1118 cm^{-1} reveals the addition of acetic acid to the active double bond of CNT surface. Furthermore, TGA analysis in N_2 atmosphere (which is not shown here) indicated a weight loss around 700 °C, which was attributed to the defunctionalization of CNT. The supported metal species interacted with these functional groups as anchoring sites and as a site of interactions [21, 33, 36, 37].

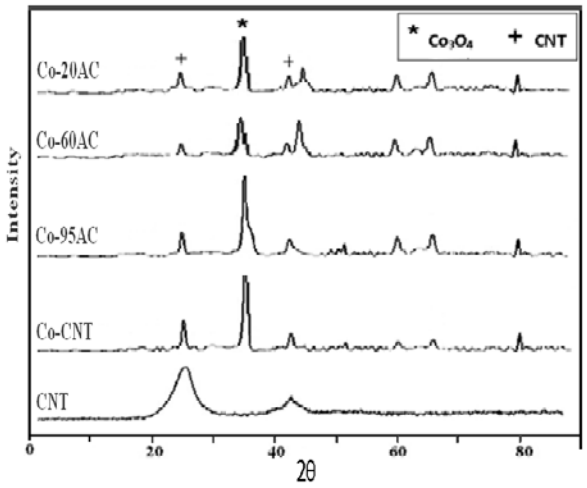

Figure 6: XRD patterns of CNT and calcined catalysts.

It was concluded that the pretreatment of CNT by acetic acid increased the carboxyl groups. On the other hand, increasing the concentrations of acetic acid caused extra the functionalization of the CNT surface, but there was an optimum concentration of acetic acid in these pretreatments according to the catalytic activity results obtained, which are reported in following paragraph.

The amount of functionalization was reversed by further increasing acetic acid concentration, which can be attributed to decreasing acetic acid dissociation constant of solvent at higher concentrations (95 vol.%). Furthermore, the dissociation constant of pretreatment solvents could change the functionalization of CNT surface. The amount of carboxyl groups for 60 vol.% acetic acid pretreatment of CNT was higher than that of 20 vol.% acetic acid. The CNT surface chemistry in Co-60Ac catalyst led to the formation of smaller supported cobalt particles. Therefore, only 60 wt.% acetic acid has the favorite balance of acetic acid concentration and dissociation constant, contributing to the formation of cobalt particles smaller in size than Co–20AC and Co–95AC as reported in Table 1.

The reducibility of the catalysts in H_2 atmosphere was determined by TPR experiments. The TPR spectra of the calcined Co-60AC, Co-20AC, Co-95AC, and Co-CNT are shown in Figure 7 and the specific reduction temperatures are presented in Table 1. The low temperature peak (300-380 °C) is typically assigned to reduction of Co_3O_4 to CoO, although a fraction of the peak likely comprises the reduction of the larger, bulk-like CoO species to CoO [22, 40, 41].

Table 1: The nomenclature, composition, TPR, TPD results, and the properties of various acetic acid modified catalysts.

Catalyst	1st TPR Peak (°C)	2nd TPR Peak (°C)	Reduction Degree(%)[a]	μ mole H_2 desorbed /gr cat.	Cobalt Dispersion (%)	XRD- $d_{Co_3O_4}$ (nm)	d_{Co^o} (nm)
Co-60AC	335	438	75	819.25	25.02	7.9	5.4
Co-20AC	350	427	68	548.77	17.29	9.7	6.7
Co-95AC	360	420	62	464.55	15.37	10.5	7.1
Co-CNT	370	450	58	312.45	11.98	11.1	7.2

[a] Determined through integration of area under TPR peaks from 40 °C to 900 °C.

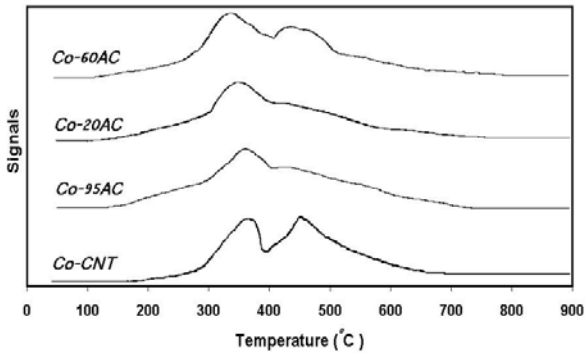

Figure 7: TPR patterns of the calcined catalysts from 40 to 900 °C.

The second broad peak is assigned to the reduction of small CoO to CoO species, which also includes the reduction of cobalt species that interact with the support.

According to Figure 7 and Table 1, the deposition of cobalt nanoparticles on acetic acid pretreated CNT shifts the reduction peaks to a lower temperature compared with the catalyst prepared by common CNT, indicating higher reducibility for high dispersion of cobalt particles produced in this special method. Interestingly, the reduction temperature of the first peak also decreases with decreasing cobalt particle size.

According to the TEM images of the catalysts prepared on acetic acid pretreated CNT, most of the small particles are inside the tubes, especially for the Co-60AC catalyst, which in turn leads to a better interaction with the internal walls of the pretreated CNT and favors the reduction of Co_3O_4 species [42, 26]. As shown in Figure 7, for the Co-95AC, Co-20AC, and Co-60AC catalysts, by decreasing the cobalt particle size, the second reduction peak shifts to higher temperatures and the broad shoulder of the second TPR peak becomes larger, suggesting more difficult reduction process for CoO species with smaller cobalt particles. Indeed, the degree of interaction with the metal phase and the support varies with the cobalt particle size; larger CoO particles are reduced more easily than smaller CoO particles [1, 29, 43].

Thus, to have a better understanding of the compared reducibility of the catalysts, the areas under the TPR peaks were calculated by integration. The areas of the peaks are proportional to the amount of H_2 consumption and attributed to the reduction degree of catalysts. Therefore, the reduction degree of the catalysts prepared on acetic acid pretreated CNT are higher than the catalyst Co-CNT. This matter can be described as follows:

Since the functional groups on the CNT surface were stable at 400 °C in air [16], it was assumed that the functional groups from acetic acid formed on the pretreated CNT surface not only obstructed the sintering of cobalt, but also promoted activating hydrogen or accelerated the hydrogen spill-over effect under the reduction process; this contributes to realizing a higher dispersion and reduction degree of these catalysts simultaneously. This hydrogen spill-over effect also shifts the TPR peaks to lower temperatures for the Co-60AC, Co-20AC, and Co-95AC catalysts compared with Co-CNT [8, 44]. In addition, in cobalt catalysts supported on the pretreated CNT, by increasing the cobalt particle size, the reduction temperature for the species (which need to be reduced at high temperatures) decreases and this suggests an easier reduction for larger cobalt particles.

As shown in Figure 7, there is no significant evidence for the formation of metal-support compounds on the catalyst surface, due to the absence of significant reduction peaks above 500 °C. Tavasoli et al. [2], as well as Martinez et al. [45], have noted that the reduction peak present at temperatures above 530 °C with an oxidic carrier shows the formation of cobalt species, which are difficult to be reduced (oxide compounds). CNT as an inert support for cobalt catalyst does not show any peak related to the formation of metal-support compounds as compared to Co/γ-Al_2O_3 catalysts, suggesting an easier reduction process with CNT than with oxidic carriers [2, 23, 24].

The results of the temperature programmed desorption (TPD) of the Co-60AC, Co-20AC, Co-

95AC, and Co-CNT catalysts are also given in Table 1. This table shows that in case of Co-60AC, Co-20AC, and Co-95AC catalysts, the hydrogen chemisorption (H_2 uptake) increases with decreasing the cobalt particle sizes up to 5.5 nm in accordance with the dispersion percentage of the cobalt particles. Thus increasing the cobalt particle size decreases the percentage of dispersion from 25.02 to 15.37 % (see Table 1).

The H_2 uptake of the Co-60AC catalyst is higher than that of the Co-CNT catalyst because of narrow particle size distributions and the confinement of cobalt nanoparticles in CNT pores, which is more efficient than particle size distributions [42, 45]. Also, this matter can be attributed to the hydrogen spill-over of the isolated CNTOH functional groups, which are stable at 400 °C [15]. Moreover, Bezemer et al. observed that H_2 uptake is directly related to particle size, a trend which levels off for larger particles [1].

The Effects of Acetic Acid Pretreatment

To investigate the promotional role of acetic acid in the pretreatment of the support, cobalt modified CNT-supported catalysts prepared by above procedure were used in the FTS reaction in a CSTR reactor for the total test run of 120 hrs. After the initial catalyst stability was reached, the results of FTS rate (gr. HC produced/gr. cat. /hr), water–gas shift reaction (WGS) rate, and the percentage of CO conversion under the reaction condition of 220 °C, 2.5 MPa, and a H_2 to CO ratio of 2 were calculated for Co-CNT, Co-60AC, Co-20AC, and Co-95AC catalysts, and all the results are reported in Table 2. FT synthesis rate is equal to the gr HC produced/gr cat./hr and WGS rate is equal to the formation rate of CO_2 (R_{FCO_2}) and can be defined by [27]:

$$R_{WGS} = R_{FCO_2} = \frac{gr.CO_2\ produced}{gr.cat.\min} \qquad (10)$$

In acetic acid pretreated CNT-supported catalysts, the WGS rate is higher than the conventional catalyst supported on common CNT. The increase of the WGS reaction rate or CO_2 formation rate can be attributed to the increase in water partial pressure, due to an increase in FTS reaction rate in the pretreated CNT-supported catalysts [2].

As shown in Table 2, Co–60AC catalyst exhibited the highest CO conversion of 52.4% in FTS reaction and the lowest selectivity of CH_4 in this study. Co–CNT catalyst showed a lower CO conversion of 45% in this study. The Co–CNT catalyst had a large cobalt particle size, leading to lower cobalt surface area and dispersion, which in turn resulted in lower catalytic activity. The synthesis of highly dispersed and stable Co catalysts requires strong interaction between the support and the Co precursor [15]. The precursor-support interaction can be raised by increasing the amount of functional groups on the surface of the support as shown by TerŐkrde for iron containing catalysts [46]. For the catalysts, prepared from acetic acid pretreated CNT supports, the different surface properties and the existence of functional groups on CNT supports contributed to the formation of small cobalt particles, which resulted in the high dispersion of the supported cobalt and lead to a high catalytic activity of these catalysts in FTS reaction, provided that the reduction degree of cobalt particles was high enough.

The comparative C_{5+} selectivity and CH_4 selectivity for the Co–20Ac, Co–60Ac, Co–90Ac, and Co–CNT catalysts show that the catalysts prepared through acetic acid pretreated CNT has a higher C_{5+} selectivity and a lower CH_4 selectivity than the C_4 catalysts. Increasing the C_{5+} selectivity can be related to the uniformity of the particle size, which improves the hydrogenation of carbon monoxide. Moreover, it can be attributed to wall electron deficiency inside the CNT, which enhances the CO chemisorption and enlarges the residence time of the reactants; thus it allows a higher probability of forming longer carbon chains. [26,31-32]. The decrease in the selectivity of CH_4 and olefin to

paraffin ratio can be explained by the effective participation of olefins in the carbon–carbon chain propagation for the uniform cobalt clusters produced in acetic acid pretreated CNT-supported cobalt catalysts.

Table 2: The reaction performance of various catalysts.

Catalyst	FTS Rate (gr. HC/gr. cat./hr)	Olefin/Paraffin ratio	CO conversion. (%)	Selectivity (%)		
				CH_4	C_5^+	CO_2
Co-60AC	0.72	0.55	52.4	7.7	88.5	1.97
Co-20AC	0.63	0.61	48.1	6.6	85.3	1.70
Co-95AC	0.64	0.69	49.3	6.4	87.1	1.83
Co-CNT	0.62	0.73	45.0	10.5	82.5	1.62

CONCLUSIONS

The promotional effects of solvent during the preparation of FTS catalysts were investigated. The acetic acid modified the support and formed new functional groups on CNT surface. The modified surface properties of CNT support realized a high dispersion and reduction degree of the supported cobalt simultaneously, contributing to high catalytic activity of this kind of catalyst applied to FTS reactions in a CSTR after the initial catalyst stability. The synthesis of highly dispersed and stable cobalt catalysts causes a strong interaction between the support and the Co precursor, resulting in the high activity and stability of this catalyst. It is found that the dilemma of dispersion and reducibility of cobalt CNT-supported catalyst will be easily resolved via reconstructing the surface properties of supports by various solvents such as acetic acid during the preparation of the catalyst. Pretreated CNT, as a catalyst support of cobalt nanoparticles, maintains the high dispersion and reducibility of cobalt, which can be attributed to hydrogen spill-over effect of functional groups on the CNT surface. This event will not normally occur for catalysts prepared by common CNT or with small particles supported on oxidic carriers. The simultaneously improved dispersion and reducibility of cobalt nanoparticles CNT-supported will contribute to the formation of more active sites on the catalysts, which is advantageous to any structure-insensitive reaction.

ACKNOWLEDGEMENTS

The authors are thankful to the Research Council of the Research Institute of Petroleum Industry (RIPI) and also to the Research and Development of the National Iranian Oil Company for their financially support of this work.

REFERENCES

[1] Bezemer G., Bitter L. J. H., Kuipers H. P. C. E., Oosterbeek H. et al., "Cobalt Particle Size Effects in the Fischer–Tropsch Reaction Studied with Carbon Nanofiber Supported Catalysts," *Journal of the American Chemical Society*, **2006**, *128*, 3956–3964.

[2] Tavasoli A., Malek Abbaslou R. M., Trepanier M., and Dalai A. K., "Cobalt Particle Size Effects in the Fischer–Tropsch Reaction Studied with Carbon Nanofiber Supported Catalysts," *Journal of the American Chemical Society*, **2006**, *128*, 3956–3964.

[3] Jacobs J. L., Zhang G. Y., Das T., and Davis B. H., "Fischer–Tropsch Synthesis: Effect of Small Amounts of Boron, Ruthenium and Rhenium on Co/TiO_2 Catalysts," *Applied Catalysis A: General*, **2002**, *223*, 195-203

[4] Dry M. E., "High Quality Diesel via the Fischer–Tropsch Process," *Journal of Chemical Technology and Biotechnology*, **2001**, *77*, 43-55.

[5] Jacobs G., Das T. K., Zhang Y., Li J., and et al., "Fischer–Tropsch Synthesis: Support, Loading, and Promoter Effects on the Reducibility of Cobalt Catalysts," *Applied Catalysis A: General*, **2001**, *233*, 263-281.

[6] Iglesia E., Soled S. L., and Fiato R. A., "Fischer-Tropsch Synthesis on Cobalt and Ruthenium. Metal Dispersion and Support Effects on Reaction Rate and Selectivity," *Journal of Catal*ysis, **1992**, *137*, 212-224.

[7] Johnson B. G., Bartholomew C. H., and Goodman D. W., "The Role of Surface Structure and Dispersion in CO Hydrogenation on Cobalt," *Journal of Catal*ysis, **1991**, *128*, 231-247.

[8] Tavasoli A., Mortazavi Y., Khodadadi A., Sadagiani K., and et al., "Effects of Different Loadings of Ru and Re on Physico-chemical Properties and Performance of 15% Co/Al_2O_3 FTS Catalysts," *Iranian Journal of Chemistry and Chemical Engineering*, **2005**, *35*, 9-17.

[9] Van Berge P. J., Van de Loosdrecht J., Barradas S., and Van Der Kraan A. M., "Oxidation of Cobalt Based Fischer-Tropsch Catalysts as a Deactivation Mechanism," *Catalysis Today*, **2000**, *58*, 321-334.

[10] Reuel R. C. and Bartholomew C. H., "Effects of Support and Dispersion on the CO Hydrogenation Activity/Selectivity Properties of Cobalt," *Journal of Catal*ysis**, 1984**, *85*, 78-88.

[11] Bezemer G. L., van laak A., van Dillen A. J., and de Jong K. P., "Cobalt Supported on Carbon Nanofibers- a Promising Novel Fischer-Tropsch Catalyst," *Studies in Surface Science and Catalysis*, **2004**, *147*, 259-264.

[12] Serp P., Corrias M., and Kalck P., "Carbon Nanotubes and Nanofibers in Catalysis," *Applied Catalysis A: General*, **2003**, *253*, 337-358.

[13] Tavasoli A., Rashidi A., Sadaghiani K., Karimi A., Khodadadi A., and Mortazavi Y., "Carbon Nanotubes Supported Cobalt Catalyst for Converting Synthesis Gas into Hydrocarbons," *European Patent*, EP 1782885**, May 9. 2007**.

[14] Guczi L., Stefler G., Geszti O., Koppany Z. et al., "CO Hydrogenation over Cobalt and Iron Catalysts Supported over Multiwall Carbon Nanotubes: Effect of Preparation," *Journal of Catal*ysis, **2006**, *244*, 24-32.

[15] Zhang Y., Liu Y., Yang G., Endo Y. et al., "The Solvent Effects during Preparation of Fischer-Tropsch Synthesis Catalysts: Improvement of Reducibility, Dispersion of Supported Cobalt and Stability of Catalyst," *Catal*ysis *Today*, **2009**, *142*, 85-89.

[16] Ho S. W. and Su Y. S., "Effects of Ethanol Impregnation on the Properties of Silica-supported Cobalt Catalysts," *Journal of Catal*ysis, **1997**, *168*, 51-59.

[17] Zhang Y., Hanayama K., and Tsubaki N., "The Surface Modification Effects of Silica Support by Organic Solvents for Fischer–Tropsch Synthesis Catalysts," *Catalysis Communications*, **2006**, *7*, 251-254.

[18] Zhang Y., Liu Y., Yang G., and Sun S., "Effects of Impregnation Solvent on Co/SiO_2 Catalyst for Fischer-Tropsch Synthesis: A Highly Active and Stable Catalyst with Bimodal Sized Cobalt Particles," *Applied Catalysis A: General*, **2007**, *321*, 79-85.

[19] Ming H. and Baker B. G., "Characterization of Cobalt Fischer-Tropsch Catalysts I. Unpromoted Cobalt-Silica Gel Catalysts," *Applied Catalysis A: General,* **1995**, *123*, 23-26.

[20] Rashidi A. M., Nouralishahi A., Khodadadi A. A., and Mortazavi Y., "Modification of Single-walled Carbon Nanotubes (SWNT) for Hydrogen Storage," *International Journal of Hydrogen Energy*, **2010**, *35*, 9489-9495.

[21] Naeimi H., Mohajeri A., Moradi L., and Rashidi A. M., "Efficient and Facile One-pot Carboxylation of Multi-walled Carbon Nanotubes by Using Oxidation with Ozone under Mild Conditions," *Applied Surface Science*, **2009**, *256*, 631-635.

[22] Karimi A., Nakhaei Pour A., Torabi F., Hatami B. et al., "Fischer-Tropsch Synthesis over Ruthenium-promoted Co/Al_2O_3 Catalyst

with Different Reduction Procedures," *Journal of National Gas Chemistry*, **2010**, *19*, 503-508.

[23] Tavasoli A., Sadagiani K., Khorashe F., and Seifkordi A. A., "Cobalt Supported on Carbon Nanotubes- A Promising Novel Fischer–Tropsch Synthesis Catalyst," *Fuel Processing Technology*, **2008**, 89, 491-498.

[24] Rashidi A. M., Karimi A., Bozorgzadeh H. R., Kashefi K. et al., "Synthesis of SWNT's over Nanoporous Co-Mo/MgO and Using as a Catalyst Support for Selective Hydrogenation of Syngas to Hydrocarbon," *Journal of National Gas Chemistry*, **2010**, *19*, 548-551.

[25] Fan L., Yokota K., and Fujimoto K., "Supercritical Phase Fischer-Tropsch Synthesis: Catalyst Pore-size Effect," *AIChE Journal*, **1992**, *38*, 1639-1648.

[26] Chen W., Fan Z., Pan X., and Bao X., J. "Effect of Confinement in Carbon Nanotubes on the Activity of Fischer–Tropsch Iron Catalyst," *Journal of the American Chemical Soc*iety, **2008**, *130*, 9414-9419.

[27] Tavasoli A., Sadaghiani K., Nakhaeipour A., Ghalbi Ahangari M. et al., "Cobalt Loading Effects on the Structure and Activity for Fischer-Tropsch and Water-gas Shift Reactions of Co/Al_2O_3 Catalysts," *Iranian Journal of Chemistry and Chemical Engineering*, **2007**, *26*, 10-16.

[28] Trepanier M., Tavasoli A., Dalai A. K., and Abatzoglou N., "Fischer–Tropsch Synthesis over Carbon Nanotubes Supported Cobalt Catalysts in a Fixed Bed Reactor: Influence of Acid Treatment," *Fuel Processing Techology*, **2009**, *90*, 367-374.

[29] Trepanier M., Tavasoli A., Dalai A. K., and Abatzoglou N., "Co, Ru and K Loadings Effects on the Activity and Selectivity of Carbon Nanotubes Supported Cobalt Catalyst in Fischer–Tropsch Synthesis," *Applied Catalysis A: General*, **2009**, *353*, 193-202.

[30] Malek Abbaslou R. M., Tavasoli A., and Dalai AK., "Effect of Pre-treatment on Physico-chemical Properties and Stability of Carbon Nanotubes Supported Iron Fischer–Tropsch Catalysts," *Applied Catalysis A: General*, **2009**, *355*, 33-41.

[31] Karimi A., Rashidi A. M., and Nasernejad B., "Synthesis and Characterization of Multi-walled Carbon Nanotubes /Alumina Nanohybrid-supported Cobalt Catalyst in Fischer-Tropsch Synthesis," *Journal of National Gas Chemistry*, **2013**, 22, 582-590.

[32] Trepanier M., Dalai A. K., and Abatzoglou N., "Synthesis of CNT-supported Cobalt Nanoparticle Catalysts Using a Microemulsion Technique: Role of Nanoparticle Size on Reducibility, Activity and Selectivity in Fischer–Tropsch Reaction," *Applied Catalysis A: General*, **2010**, *374*, 79-86.

[33] Talaei Z., Mahjoub A. R., Rashidi A. M., Amrollahi A. et al., "The Effect of Functionalized Group Concentration on the Stability and Thermal Conductivity of Carbon Nanotube Fluid as Heat Transfer Media," *International Communication in Heat and Mass Transfer*, **2011**, *38*, 513-517.

[34] Bronnimann C. E., Chuang I. S., Hawkins B. L., and Maciel G. E., "Dehydration of Silica-aluminas Monitored by High-resolution Solid-state Proton NMR," *Journal of The American Chemical Society*, **1987**, *109*, 1562-1564.

[35] Bronnimann C. E., Zeigler R. C., and Maciel G. E., "Proton NMR study of Dehydration of the Silica Gel Surface," *Journal of The American Chemical Society*, **1988**, *110*, 2023-2026.

[36] Qu Z., Huang W., Zhou S., Zheng H. et al., "Enhancement of the Catalytic Performance of Supported-metal Catalysts by Pretreatment of the Support," *Journal of Catal*ysis, **2005**, *234*, 33-36.

[37] Uchino T., Aboshi A., Kohara S., Ohishi Y., et al., "Microscopic Structure of Nanometer-sized Silica Particles," *Physical Review B*, **2004**, *69*, 155409.

[38] van Steen E., Sewell G. S., Makhothe R. A., Micklethwaite C. et al., "TPR Study on the Preparation of Impregnated Co/SiO_2 Catalysts," *Journal of Catal*ysis, **1996**, *162*, 220-229.

[39] Sun S., Tsubaki N., and Fujimoto K., "The Reaction Performances and Characterization

of Fischer–Tropsch Synthesis Co/SiO_2 Catalysts Prepared from Mixed Cobalt Salts," *Applied Catalysis A: General*, **2000**, *202*, 121-131.

[40] Huffman G. P., Shah N., Zhao J., Huggins F. E., Hoost T. E., and et al., "In-Situ XAFS Investigation of K-promoted Co Catalysts," *Journal of Catal*ysis, **1994**, *151*, 17-25.

[41] Lin H. Y. and Chen Y. W., "The Mechanism of Reduction of Cobalt by Hydrogen," *Material Chemistry and Physics*, **2004**, *85*, 171-175.

[42] Pan X., Fan Z., Chen W., Ding Y. et al., "Enhanced Ethanol Production inside Carbon-Nanotube Reactors Containing Catalytic Particles," *Nature Materials*, **2007***, 6*, 507–511.

[43] Bezemer G. L., Radstake P. B., Koot V., van Dillen A. J. et al., "Preparation of Fischer-Tropsch Cobalt Catalysts Supported on Carbon Nanofibers and Silica Using Homogeneous Deposition-precipitation," *Journal of Catal*ysis, **2006**, *237*, 291-302.

[44] Das T. K., Jacobs G., Patterson P. M., Conner W. A. et al., "Fischer-Tropsch Synthesis: Characterization and Catalytic Properties of Rhenium Promoted Cobalt Alumina Catalysts," *Fuel*, **2003**, *82*, 805-815.

[45] TerÖrde R. J. A. M., Ph.D. Thesis, Utrecht University, Utrecht, the Netherlands, **1996**.

[46] Allison J. N., Goddard III W. A., "Oxidative Dehydrogenation of Methanol to Formaldehyde," *Journal of Catal*ysis, **1985**, *92*, 127-135.